Original Research

Comparison of Parallel Acquisition Techniques Generalized Autocalibrating Partially Parallel Acquisitions (GRAPPA) and Modified Sensitivity Encoding (mSENSE) in Functional MRI (fMRI) at 3T

Christine Preibisch, PhD,[1]* Tim Wallenhorst,[1] Robin Heidemann, PhD,[2] Friedhelm E. Zanella, MD,[3] and Heinrich Lanfermann, MD[3]

Purpose: To evaluate the parallel acquisition techniques, generalized autocalibrating partially parallel acquisitions (GRAPPA) and modified sensitivity encoding (mSENSE), and determine imaging parameters maximizing sensitivity toward functional activation at 3T.

Materials and Methods: A total of eight imaging protocols with different parallel imaging techniques (GRAPPA and mSENSE) and reduction factors (R = 1, 2, 3) were compared at different matrix sizes (64 and 128) with respect to temporal noise characteristics, artifact behavior, and sensitivity toward functional activation.

Results: Echo planar imaging (EPI) with GRAPPA and a reduction factor of 2 revealed similar image quality and sensitivity than full *k*-space EPI. A higher incidence of artifacts and a marked sensitivity loss occurred at R = 3. Even though the same eight-channel head coil was used for signal detection in all experiments, GRAPPA generally showed more benign patterns of spatially-varying noise amplification, and mSENSE was also more susceptible to residual unfolding artifacts than GRAPPA.

Conclusion: At 3T and a reduction factor of 2, parallel imaging can be used with only little penalty with regard to sensitivity. With our implementation and coil setup the performance of GRAPPA was clearly superior to mSENSE. Thus, it seems advisable to pay special attention to the employed parallel imaging method and its implementation.

Key Words: fMRI; parallel imaging; GRAPPA; mSENSE; fMRI sensitivity; artifact behavior
J. Magn. Reson. Imaging 2008;27:590–598.

IN RECENT YEARS, MRI, and even more, functional MRI (fMRI), have shown a strong trend toward higher field strengths (1,2). Associated with this is the desire to achieve higher sensitivity toward functional activation as well as increased spatial resolution. However, this requires still higher gradient power, leading to tremendous acoustic noise (3) and a considerable increase in helium boil off. Moreover, susceptibility artifacts are a more serious problem at 3T than at 1.5T. A potential solution is the application of parallel acquisition strategies (4–7), which employ the spatially-varying sensitivities of surface coil arrays for spatial encoding and concomitantly allow an undersampling in *k*-space. For Cartesian trajectories, this corresponds to a reduction of the number of phase-encoding (PE) steps. This either allows the significant reduction of susceptibility artifacts like distortions and blurring (8–17), or the mitigation of gradient acoustic noise (4). Since the first method demonstrating in vivo results, termed simultaneous acquisition of spatial harmonics (SMASH), was developed primarily for cardiac imaging (18) a multitude of parallel imaging techniques have been developed (5), but only three of them, namely sensitivity encoding (SENSE) (19), modified SENSE (mSENSE) (20), and generalized autocalibrating partially parallel acquisitions (GRAPPA) (21), are commercially available on MR scanners.

The primary difference between these methods lies in the image reconstruction process for undersampled reduced field-of-view (FOV) data, which either consists of an unfolding procedure in image space (SENSE) or is based on the calculation of missing *k*-space data prior to the image reconstruction (GRAPPA). During SENSE reconstruction, a reduced FOV image is generated for each component coil. Each pixel in these reduced FOV images contains signal contributions from R (reduction factor) different positions in the full FOV image, which

[1]Brain Imaging Center, University Frankfurt, Frankfurt, Germany.
[2]Siemens Medical Solutions, Erlangen, Germany.
[3]Institute of Diagnostic and Interventional Neuroradiology, Hannover Medical School.

Contract grant sponsor: Bundesministerium für Bildung und Forschung (Brain Imaging Center Frankfurt); Contract grant number: DLR 01GO0203; Contract grant sponsor: Deutsche Forschungsgemeinschaft; Contract grant number: ZA 233/1-1.

*Address reprint requests to: C.P., Brain Imaging Center, University Frankfurt, Schleusenweg 2-16, D-60528 Frankfurt, Germany.
E-mail: preibisch@em.uni-frankfurt.de

Received January 2, 2007; Accepted September 4, 2007.
DOI 10.1002/jmri.21191
Published online 24 January 2008 in Wiley InterScience (www.interscience.wiley.com).

need to be separated. The unfolding algorithm is based on the fact that in each single coil image, superposition occurs with different weights according to the local coil sensitivities. Assuming that an *N*-element phased array coil was used for signal reception, the signal superposition in all folded single-coil images can be described by a system of *N* linear equations. The reconstruction process essentially requires the solution of this set of *N* linear equations for all pixel positions in the folded image. To achieve this, proper coil sensitivity information is necessary, which is obtained from an additional low-resolution full FOV reference scan. GRAPPA, on the other hand, calculates missing data points in *k*-space by means of a specialized fitting procedure. In contrast to SMASH and SENSE, it does not require detailed information on coil sensitivities. Instead, it acquires a few additional *k*-space lines (autocalibration signals [ACS]) prior to each image acquisition. These ACS lines are then used to determine the weights that are needed to reconstruct the missing lines in *k*-space for each coil. This is done by fitting multiple lines from all component coils to an ACS line acquired in a single coil of the array. In this way, the missing *k*-space lines are determined for each component coil separately. A Fourier transform can then be used to generate an uncombined image for each component coil. These full FOV component coil images can then be combined by a sum of squares algorithm. The use of multiple *k*-space lines from all coils to fit one single coil ACS line results in an increased accuracy of the fit procedure. The sum of squares combination of single coil images increases signal-to-noise ratio (SNR) and avoids phase cancellations as well as low SNR, which are general drawbacks of previous *k*-space–based parallel imaging methods. SENSE and GRAPPA both work with arbitrary coil configurations as long as the coil sensitivities vary in the PE direction in which the reduction is performed. However, the SNR or spatially-variable noise amplification depends on the coil geometry, which can be described by the geometry factor *g*. Even though the *g*-factor represents a quantitative estimation of noise enhancement only for SENSE (19), Griswold (22) found that the *g*-factor also describes spatially variable noise amplification for GRAPPA since both methods have the same requirements with regard to coil configuration. mSENSE (20) denotes a modification that maintains the image-based reconstruction process of the original SENSE method but uses an autocalibration acquisition modus resembling GRAPPA. The required coil sensitivity maps are generated from a few additional integrated ACS lines. Additionally, a set of noise scans are acquired for calculation of the noise correlation matrix that is used in the modified SENSE reconstruction process. For echo planar imaging (EPI) time series as used for fMRI, the additional ACS lines are acquired only once before the beginning of the actual time series. Details on the reconstruction algorithms of the different methods, and their assets and drawbacks can be found in the original publications of the respective methods (19–21) and in a recent review by Blaimer et al (5).

As far as fMRI applications are concerned, SENSE is already quite widely used while, at least to our knowledge, there is only quite limited experience with GRAPPA (15,23). Therefore, two quite comprehensive reviews by Golay et al (6) and de Zwart et al (7) on technical issues as well as the potential of parallel imaging in fMRI concentrate on SENSE. Up to now, SENSE was either used to increase spatial resolution (24,25), mitigate susceptibility artifacts like distortions and blurring (10–17), or reduce gradient acoustic noise (4). Most studies indicate that the related sensitivity losses in fMRI are generally smaller than could be expected from the concomitant loss in SNR alone. In an earlier study at 1.5T it could be shown that SENSE-EPI at a reduction factor (R) of 2 and constant readout bandwidth (BW) allows one to substantially reduce image distortions and blurring while time-course SNR and statistical power were hardly affected (26). Also, theoretical indications that at higher magnetic field strengths the transition from optimal to deteriorating imaging performance takes place at an increased R (27,28) are supported by some abstracts reporting experimental data for SENSE (12,14,15,29). In a more comprehensive recent study, Schmidt et al (17) demonstrated that at 3T SENSE, reduction factors higher than 2 can improve image quality and statistical power in some areas (occipital lobe and fusiform gyrus) but not in others (medial temporal lobe). This inhomogeneous sensitivity profile could be expected from the spatially-varying noise amplification and suggests that imaging parameters have to be optimized for each particular fMRI study with respect to the brain areas of interest. However, it might well be that different parallel imaging methods per se show an overall more or less favorable behavior but there is, at least to our knowledge, no practical experience using other parallel imaging methods in fMRI applications.

The goal of this study was therefore to evaluate the parallel imaging techniques GRAPPA and mSENSE for their respective performance in functional imaging studies. To clarify whether it is more beneficial to use stronger gradients or parallel imaging approaches to realize a certain spatial resolution and TE, we compared eight imaging protocols with different parallel imaging techniques, reduction factors, and matrix sizes at the respective minimum BWs. The comparison was performed with respect to artifact behavior, noise characteristics (temporal SNR), and sensitivity toward functional activation in a simple visual task.

MATERIALS AND METHODS

MRI Hardware

Imaging was performed on a 3T Siemens Magnetom Trio MR scanner (Siemens Medical Solutions, Erlangen, Germany). The maximum gradient strength and slew rate were 40 mT/m and 200 T/m/second, respectively. For parallel imaging of the head, the system is equipped with an eight-channel receive-only head coil (MRI Devices Corporation, Waukesha, WI, USA) whose elements are connected to eight independent receiver channels, and the body coil is used for signal transmission. The parallel imaging performance of the coil at different reduction factors (R) can be characterized by a mapping of the inverse geometry factor ($100 \times 1/g$); an

example is shown in Fig. 1 for R = 2 and 3, axial slice orientation, and PE in the anterior–posterior direction.

Imaging Protocols

A total of eight single-shot EPI imaging protocols, covering two different parallel imaging techniques (GRAPPA and mSENSE), three different reduction factors (R = none, 2, 3), and two different spatial resolutions ($3 \times 3 \times 3\ mm^3$ or $2 \times 2 \times 2\ mm^3$) were performed. The TE were 30 msec and 35 msec with base resolutions of 64 and 128, respectively. To achieve a TE of 35 msec at base resolution 128 without parallel imaging it was necessary to trim the number of lines in the PE direction, which was anterior–posterior. Therefore, a partial Fourier technique was used to reduce the number of measured PE lines to seven-eighths (effective matrix size 128×112) for all high-resolution protocols. A comparison of different partial Fourier methods can be found, e.g., in Ref. 30. To achieve a repetition time (TR) of 2.55 seconds in each case, we acquired 36 slices with base resolution 64 and 25 slices with base resolution 128. The slices were positioned almost axially along the anterior commissure-posterior commissure line. Since it was the goal of the study to investigate whether parallel imaging could be used to reduce gradient strain and thus acoustic noise and helium boil off, the BW was always adjusted to the minimum value, keeping the total readout duration, i.e., the length of the echo train, about constant. Since the reference lines used for autocalibration were acquired in a separate fast EPI prescan, the number of references lines was always set to the maximum possible value. For the complete set of imaging parameters see Table 1.

Subjects and Stimulation Protocol

A total of 11 healthy volunteers (six male, five female; mean age 28.8 ± 6.4 years, range 21–42 years) gave written informed consent before participating in the study. The complete program of eight single-shot EPI imaging protocols was performed in three volunteers. Six volunteers were only subjected to the high-resolution protocols, two volunteers only to the low-resolution protocols. For each protocol a total of 60 scans were acquired during three cycles of alternating rest and visual stimulation (alternating black and white checkerboard). Subjects were asked to fixate on a central spot during all fMRI runs. To avoid an inherent bias due to the chronological order of the experiments, their succession was permutated randomly.

Data Analysis

Custom software written in MATLAB (The MathWorks, Inc., Natick, MA, USA) was used to evaluate time course stability by a pixel-wise calculation of SNR over the time course (temporal SNR): $SNR(t) = \langle S(t) \rangle / \sigma(t)$, where $\langle S(t) \rangle$ denotes the average and $\sigma(t)$ the SD of signal over an individual pixel time course. For each experiment, median values of temporal SNR were determined from all pixels within the brain and averaged over the subjects. This allows assessing time course stability, which is the most important prerequisite for high-quality fMRI experiments. The details and rationale of the analysis were described previously (26). To assess the influence of parallel imaging on the temporal SNR, the subjects averages (±SD) were compared to a theoretical estimation for the SNR change that was derived from the

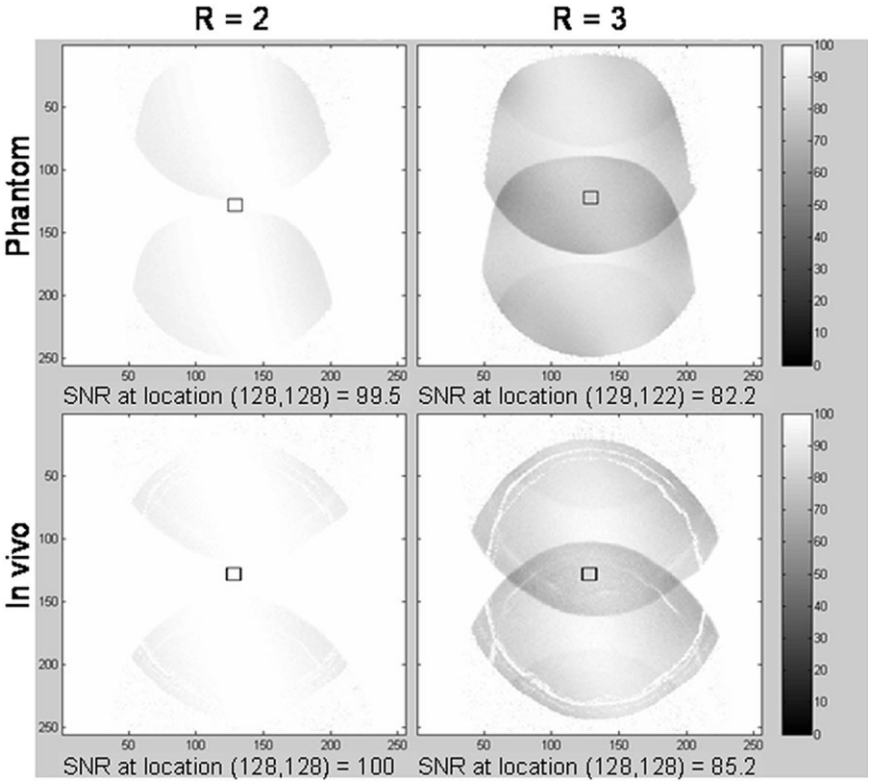

Figure 1. Parallel imaging performance of an eight-channel head coil (identical to that used in the presented experiments). The maps of the inverse geometry factor ($100 \times 1/g$) demonstrate spatially-variable noise amplification due to geometric properties of the coil in a head phantom (top row) and a human subject (bottom row) at 3T for R = 2 (left column) and R =3 (right column) for axial slice orientation and anterior–posterior PE direction (Courtesy of Siemens Medical Solutions). One can see that noise amplification not only depends on the reduction factor but also on the object. Thus, the geometry factor is not simply characteristic for a specific coil but also depends on coil load.

Table 1
Details on Acquisition Parameters (Bandwidth, Readout Duration Per Echo, Echo Spacing, Number of Reference Lines, Number of Subjects) and Subject Averages (± SD Over Subjects) for Median (SNR(t)), Maximum t-Value at Pixel Level, and Cluster Size for Different Spatial Resolutions, Parallel Imaging (PI) Methods, and Reduction Factors (as Indicated in Top Row)

	Voxel size							
	$3 \times 3 \times 3$ mm^3, matrix size = 64×64			$2 \times 2 \times 2$ mm^3, base resolution = 128				
PI method R	None	GRAPPA 2	mSENSE 2	None	GRAPPA 2	GRAPPA 3	mSENSE 2	mSENSE 3
BW (Hz/pixel)	1420	752	752	1860	1056	752	1056	752
Readout duration (μsec)	704	1330	1330	538	947	1330	947	1330
Echo spacing (μsec)	770	1430	1430	600	1030	1420	1030	1420
N refs		31	31		55	75	55	75
N subjects	5	5	5	9	9	8	9	8
Median of SNR (t)	60.0 ± 12.1	52.4 ± 15.8	48.8 ± 13.3	37.2 ± 7.8	33.7 ± 8.1	33.8 ± 6.8	26.0* ± 5.1	23.6* ± 7.4
Theory	60.0	58.3	58.3	37.2	35.8	33.8	35.8	33.8
Maximum t-value	22.5 ± 6.5	18.5 ± 8.3	22.1 ± 6.4	24.5 ± 3.2	23.7 ± 4.4	18.7 ± 8.2	22.3 ± 5.0	19.4* ± 4.0
Cluster size (number of voxels)	6762 ± 3351	4744 ± 3125	5074 ± 2740	4890 ± 1200	4255 ± 1509	3258* ± 2321	4105 ± 1848	2658* ± 1446

*Significantly different from the baseline experiment without parallel imaging (paired t-test, $P < 0.05$).

dependence of purely thermal SNR on matrix ($N_xN_yN_z$) and voxel ($\Delta x\Delta y\Delta z$) size, acquisition BW and reduction factor (R): $SNR \propto \Delta x\Delta y\Delta z/(\sqrt{R \cdot BW/(N_xN_yN_z)})$. Actually, with parallel imaging there is an additional spatially variable noise amplification that depends on coil geometry. For SENSE, this noise component was described by a geometry factor g ($SNR \propto 1/g$) (19), which is also applicable to GRAPPA (22). Since the geometry factor g is inhomogeneous throughout an entire data set and also depends on coil load as well as the actual orientation of the imaging plane (for illustration see Fig. 1), it can not easily be approximated by a single number. Thus, it was neglected, assuming ideal conditions. To avoid spurious influences of spatial resolution, which is expected to reduce SNR to about 50% when changing from base resolution 64 to 128 with the imaging parameters employed in this study, we scaled the theoretical prediction with the baseline experiments without GRAPPA for low and high spatial resolution separately.

Statistical analysis was performed using SPM2 (Wellcome Department of Cognitive Neurology, London, UK; http://www.fil.ion.ucl.ac.uk). Spatial preprocessing comprised motion correction, normalization into a standardized neuroanatomical space, and smoothing using isotropic 4-mm or 6-mm Gaussian kernels for the voxel sizes $2 \times 2 \times 2$ mm^3 and $3 \times 3 \times 3$ mm^3, respectively. Low-frequency fluctuations were removed by a high-pass filter with a cutoff at 128 seconds. For each individual subject, statistical parametric maps of t-values (SPM(t)) were created, and maximum t-values at the pixel level as well as extent (cluster size) were averaged over subjects to allow for a sensitivity comparison between the different experiments.

To test for significant differences in temporal SNR, maximum t-values, and cluster sizes, the median values of single subjects for experiments with different parallel imaging methods and reduction factors were compared by means of paired t-tests to the baseline experiments without parallel imaging at the respective spatial resolution. A particular difference was considered to be significant at $P < 0.05$.

RESULTS

Artifact Behavior

Figure 2 shows a best-case (top row) and a worst-case (bottom row) example of single slices taken from whole-brain EPI data sets of two subjects for different parameter settings. It is worth noting that all images show a

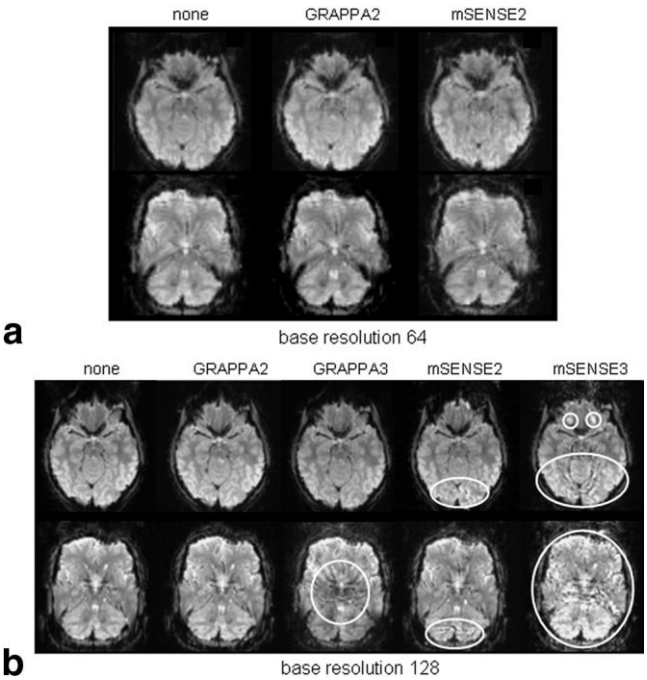

Figure 2. Image quality for experiments with different base resolution 64 (**a**) or base resolution 128 (**b**), parallel imaging method (GRAPPA or mSENSE), and reduction factor (none, 2 or 3). The two rows show single slices from two different subjects where the top row represents a best-case example and the bottom row a worst-case example. Note: images with base resolution 128 were magnified and the clipping adjusted to facilitate comparison with the low-resolution images. Areas showing significant artifacts are encircled by white ovals.

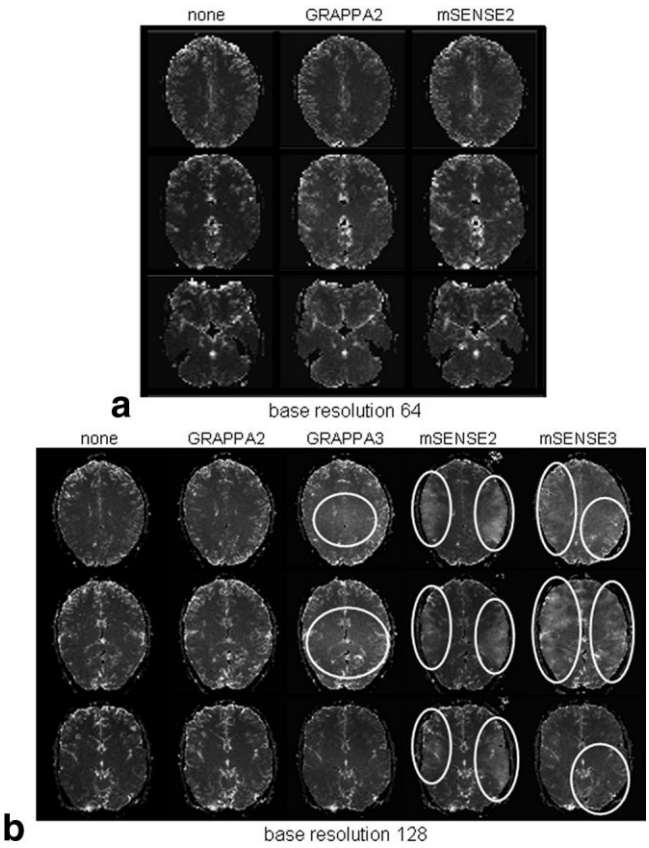

Figure 3. Images of temporal SD ($\sigma(t)$) for experiments with different base resolution 64 (**a**) and base resolution 128 (**b**), parallel imaging method (GRAPPA or mSENSE), and reduction factor (none, 2 or 3). The images are taken from a subject with overall quite benign artifact behavior. The images for different base resolutions do not show identical slices since the 36 slices acquired with base resolution 64 cover a larger brain volume than the 25 slices at base resolution 128. Note: images with base resolution 128 were magnified and the clipping adjusted to facilitate comparison with the low-resolution images. Areas with increased SD are encircled by white ovals.

similar level of susceptibility artifacts such as distortions, blurring, and signal loss. This is expected because concomitantly to increasing the reduction factor, the acquisition BW was reduced, which resulted in approximately constant echo train length at different reduction factors. With regard to residual unfolding artifacts, one can clearly see that the most serious artifacts occurred with mSENSE at a reduction factor of 3 (R = 3) while the images with GRAPPA at a reduction factor of 2 (R = 2) and in most cases (see Fig. 2, top row) even at R = 3 did not show any additional artifacts.

Noise Characteristics

The spatial distribution of temporally-varying noise as described by the temporal SD ($\sigma(t)$) depended on base resolution, parallel imaging method, and reduction factor. Figure 3 shows images of the temporal SD ($\sigma(t)$) for all eight experiments in three representative slices taken from one subject. Even though these experiments were virtually free from residual unfolding artifacts, one can readily recognize a substantial spatially-varying noise amplification that increases with the reduction factor and is worse with mSENSE as compared to GRAPPA. While at base resolution 64 the most obvious differences in noise characteristics occurred in slices near the skull base, at base resolution 128 temporal noise was clearly enhanced throughout the whole data set, especially at R = 3 and mSENSE. As can be seen in the example depicted in Fig. 3b, GRAPPA at R = 3 usually exhibited quite diffuse noise amplification in the center of the brain, which is in line with the expected noise amplification because of an increased *g*-factor in the center of the brain (see Fig. 1). mSENSE, on the other hand, gave rise to more distinct patterns. At R = 2 areas of noise amplification were located mainly laterally in frontoparietal and temporal areas; at R = 3 these areas got more widespread and formed clustered patterns throughout the brain. In experiments with severe unfolding artifacts, the temporal SD was additionally increased in affected areas.

A global assessment of SNR deterioration offers the whole-brain median of temporal SNR summarized in Fig. 4 and Table 1. To concentrate on the influence of parallel imaging instead of spatial resolution, the subject averages (±SD) are presented together with a theoretical estimation for the SNR change (derived for purely thermal noise) for low (Fig. 4a) and high (Fig. 4b) spatial resolution separately (see Materials and Methods). The neglect of the geometry factor in the theoretical calculation resulted in a relatively constant SNR in both cases, since the 1/R signal loss with parallel imaging was almost compensated for by the concomitant reduction in BW.

Deviating from the simplified theoretical prediction, only incorporating purely thermal noise, the measured median of temporal SNR showed a decrease from experiments with no parallel imaging to GRAPPA and mSENSE. At base resolution 64, the median of the temporal SNR of experiments with GRAPPA and mSENSE was on average 10% and 16% lower than expected under ideal conditions. However, these differences to the experiment without parallel imaging were not statistically significant at $P < 0.05$ (paired *t*-test). At base resolution 128, the temporal SNR was only 6% or not at all lower than expected under ideal conditions for experiments with GRAPPA at R = 2 and 3, respectively. For mSENSE on the other hand, it was even 27% and 30% lower at R = 2 and 3, respectively. When compared statistically (paired *t*-test) to the baseline experiment without parallel imaging, the temporal SNR of the experiments was significantly lower for mSENSE (P = 0.004 and 0.005 at R = 2 and 3, respectively) but not for GRAPPA.

Sensitivity Toward Functional Activation

With respect to statistics, the intersubject variability was quite high, which is mirrored by sizeable SD (Fig. 5; Table 1). At base resolution 128 the subject averages of maximum *t*-values (Fig. 5a) showed a slight decrease from no parallel imaging to GRAPPA and mSENSE both at R = 2. But there was a more pronounced reduction of maximum *t*-values at R = 3 irrespective of parallel imaging method (see Table 1). A statistical comparison

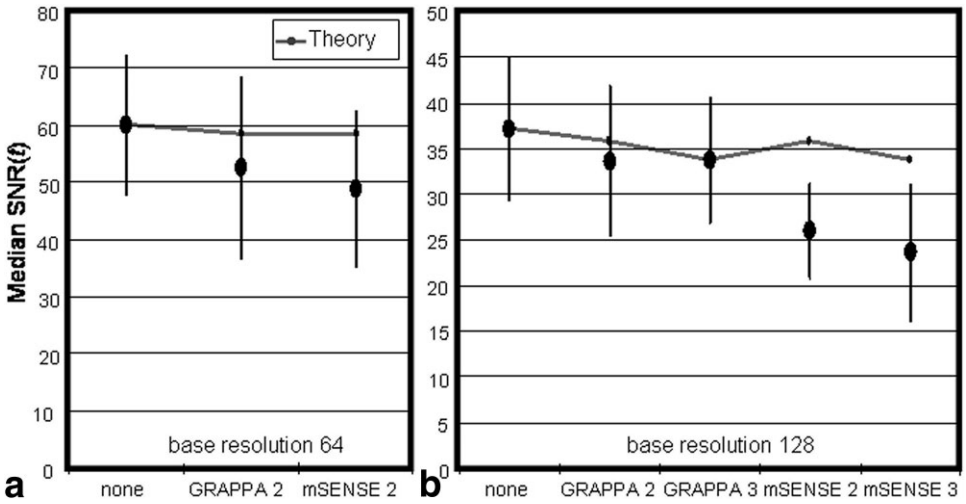

Figure 4. Whole-brain median of temporal SNR (SNR(t)) for the eight different protocols with base resolution 64 (**a**) and base resolution 128 (**b**). x-Axis labels indicate parallel imaging method and reduction factor. Error bars indicate SD over subjects. Note: Individual data points represent different numbers of subjects (see Table 1). Theoretical reference values assuming uncorrelated thermal (white Gaussian) noise (see Materials and Methods) were scaled to the protocols without parallel imaging at base resolutions 64 and base resolution 128, separately. For practical reasons, spatially-variable noise amplification as described by the geometry factor g was neglected (see Materials and Methods).

(paired t-test) revealed that the difference to the baseline experiment without parallel imaging was only significant at R = 3 for mSENSE (P = 0.01) but not for GRAPPA (P = 0.07). At base resolution 64, on the other hand, the maximum t-values of the experiments with mSENSE almost resembled those of the experiments with full k-space while the t-values of the GRAPPA experiments were clearly lower. However, this difference was not significant (paired t-test, $P < 0.05$).

Also with cluster size (see Fig. 5b; Table 1) the inter-subject variability and thus SDs over subjects were quite large. Without prejudice, subject averages showed a steady decrease from low to high spatial resolution. Furthermore, there was a decrease from no parallel

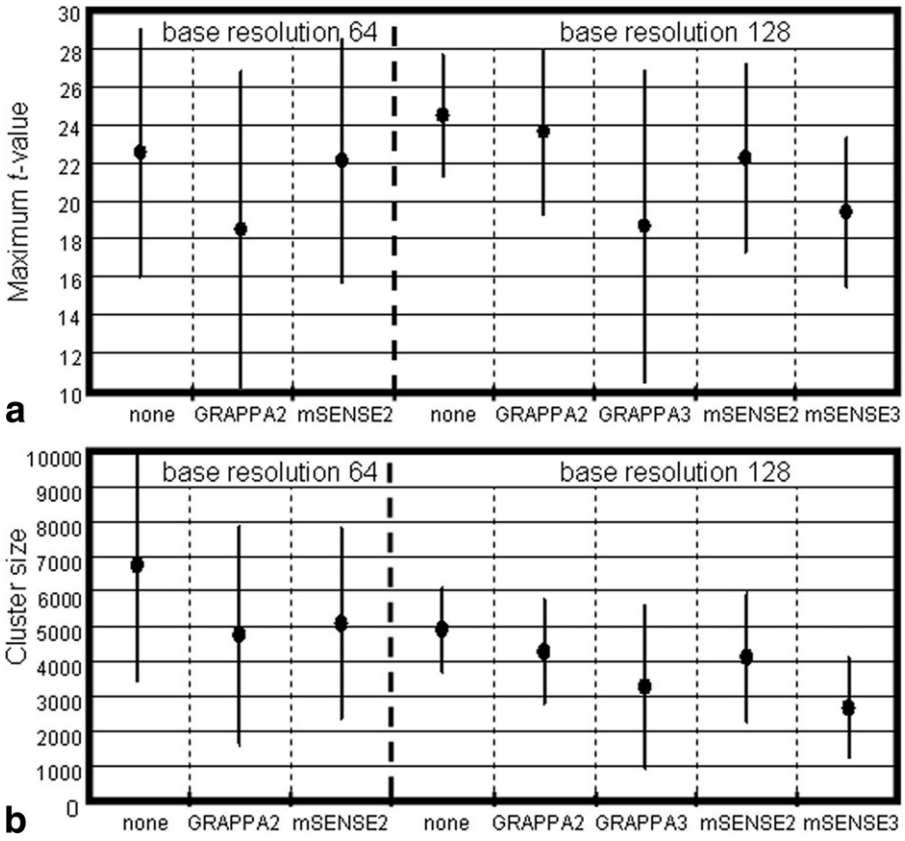

Figure 5. Subject averages of maximum t-values (**a**) and cluster size (**b**) in the visual cortex for the eight different protocols. x-Axis labels indicate parallel imaging method and reduction factor. Error bars indicate SD over subjects. Note: Individual data points represent different numbers of subjects (see Table 1).

imaging to R = 2 which continued to R = 3. However, only the cluster sizes at base resolution 128 with GRAPPA and mSENSE at R = 3 were significantly different to the experiment without parallel imaging (paired *t*-test, $P = 0.05$ and 0.005, respectively).

DISCUSSION

To some extent the current results resemble those of an earlier study at 1.5T (26), especially with regard to the fact that a reduction factor of 2 yields quite comparable results at least with GRAPPA. However, with respect to the quite different artifact behavior of GRAPPA and mSENSE, it also becomes clear that in addition to the fraction of measured data, the parallel imaging method, and also its specific implementation, plays an important role.

GRAPPA showed an optimal performance without noticeable unfolding artifacts. In comparison, mSENSE was more susceptible to reconstruction artifacts. This behavior is in agreement with the specification of the vendor, which recommends the use of the GRAPPA technique for EPI imaging. The difference in the performance of GRAPPA and mSENSE in the special case of single-shot EPI might be explained by the autocalibration approach. In general, the SENSE performance relies upon an accurate knowledge of the coil sensitivities. For a proper SENSE reconstruction, it is essential to obtain coil sensitivities without distortions and artifacts. Whenever there is a mismatch between the underlying real coil sensitivities and the derived coil sensitivities, the SENSE reconstruction will fail. In comparison, the GRAPPA method is not affected by this effect; therefore, it is possible to use, for example, a single-shot EPI sequence for autocalibration. A description of the different approaches to obtain coil sensitivity information can be found in the recent review by Griswold et al (31). Obviously, in the current study, the residual artifacts with mSENSE in individual subjects were prohibitive for functional activation studies.

Irrespective of that, the inability of SENSE and probably also mSENSE to deal with aliasing in the full FOV images (32) makes it prone to operator-induced artifacts, all the more since a FOV = 19.2 cm is a relatively common choice to achieve a voxel size of $3 \times 3 \times 3$ mm^3 with a matrix size of 64×64, and human heads often are just a few millimeters larger in the anterior–posterior direction. In this respect, it is interesting that at the lower spatial resolution the artifacts in most cases seemed to be more benign. Especially since at low spatial resolution the 19.2 cm FOV lead to small aliasing artifacts in several subjects. The reconstruction process seems to work better when less missing data have to be reconstructed. This is compatible with the finding that residual unfolding artifacts are always more severe at higher reduction factors (16). Additionally, the performance might be improved because the SNR is clearly higher, and a lower resolution also implies a shorter readout train, which reduces susceptibility artifacts and thus leads to better mSENSE reconstructions. In any case, the fact that the temporal SNR at base resolution 64 and R = 2 was considerably lower than expected under ideal circumstances is a clear indication that nevertheless some additional noise amplification occurred. Probably the artifacts are just too blurred to be clearly recognizable.

A comparison of the images of temporal SD (see Fig. 3) with the maps of the inverse *g*-factor (see Fig. 1) reveals that the patterns of noise amplification observed with GRAPPA fit quite nicely with the expected patterns due to the geometric properties of the coil. However, this is not true for mSENSE, which shows quite different patterns of noise amplification with maxima in lateral instead of central brain areas. In fact, the geometry factor depends on slice orientation and requires the existence of different coil elements along the direction in which a reduction in PE steps is desired (19,21). However, for small axial–coronal angles, as used in this study, we would not expect dramatic changes. Moreover, GRAPPA and mSENSE protocols were, except for the parallel imaging method, absolutely identical, thus, the different patterns of noise amplification must be due to the different reconstruction algorithm. Since this kind of noise amplification was not observed in an earlier study regarding SENSE-EPI (26), we assume that this can also be explained by the different implementation of the mSENSE reconstruction.

With regard to the global properties of temporal SNR, GRAPPA at base resolution = 128 showed nearly optimum performance, while for mSENSE the subject averages of the median of temporal SNR generally remained below the theoretical prediction for purely thermal noise. One might object that we could not expect to detect an SNR advantage since the theoretical calculation was based on the unrealistic ideal case with no additional noise amplification—the geometry factor *g* was assumed to be 1. But the same assumption was made in a previous study (26) and the temporal SNR then was nevertheless significantly higher than expected under ideal circumstances. This finding was confirmed by others (10,11,17) and could be explained by a decreasing contribution of physiological noise with decreasing signal strength (33,34). Another argument is that the shortening of the echo train diminishes the amount of noise that is sampled in the fringes of *k*-space (10).

However, there are obvious differences to this earlier study (26). First, the echo train length was almost constant because of the concomitant BW reduction, and the temporal SNR was therefore expected to be almost constant at a definite base resolution. This means we could not benefit from a decreasing contribution of physiological noise since at constant spatial resolution the signal strength was actually not decreasing (33,34). Also, we sampled the same amounts of noise in the outskirts of *k*-space with and without parallel imaging because the echo train length was approximately constant. Furthermore, the FOV at base resolution = 64 was considerably smaller and was in many cases quite tight-fitting, which probably led to some additional artifacts with mSENSE (32), which probably could not be directly identified because of the somewhat blurred appearance of the low-resolution images.

The fact that the temporal SNR for GRAPPA and mSENSE was rather lower than ideally expected (see Fig. 4) is a clear indication that the geometry factor

actually was higher than 1 in all experiments (see also Fig. 1), which is not really a surprise. However, at base resolution 128, the experiments with GRAPPA at R = 2 and 3 showed nearly optimum performance, while with mSENSE the temporal SNR was significantly lower than in the experiment without parallel imaging. The minor difference between GRAPPA and mSENSE at base resolution 64 might be attributed to additional artifacts caused by the tight FOV in mSENSE (32). However, at base resolution 128 the FOV is large enough by far. Thus, the marked differences between mSENSE and GRAPPA can only be explained by the different performance of the mSENSE reconstruction algorithm in the special case of single-shot EPI acquisitions, which manifests in an overall increased level of temporally-variable residual unfolding artifacts.

As far as the statistical results are concerned, it is quite obvious that a reduction factor of 3 clearly reduces sensitivity toward functional activation. Statistical comparisons (paired *t*-tests) to the baseline experiment without parallel imaging showed significant (see Table 1) or almost significant decreases in maximum *t*-values (23% and 21%) as well as cluster sizes (33% and 46%) for GRAPPA and mSENSE, respectively. At R = 2 the decreases in cluster size by 29% and 25% at base resolution 64, and by 13% and 15% at base resolution 128 for GRAPPA and mSENSE, respectively, was not significant (at $P < 0.05$), which agrees well with recent results of Lütcke et al (23) who found a decrease in the mean number of activated voxels by 21% at voxel size $2 \times 2 \times 2$ mm^3 and by 15% at voxel size $3 \times 3 \times 3$ mm^3 with GRAPPA and R = 2. This means there is a decrease in the extent of activation with parallel imaging even at R = 2 but it appears insignificant when compared to the high intersubject variability. However, one has to take into account that these results were obtained in the visual cortex, where parallel imaging does not bear any advantages. More difficult is the influence of the parallel imaging method. While at base resolution 128, subject averages of maximum *t*-values and cluster sizes were marginally higher for GRAPPA, slightly larger clusters and even clearly higher maximum *t*-values were obtained with mSENSE at voxel size $3 \times 3 \times 3$ mm^3. However, taking into account the enormous inter- and intrasubject variations, one has to be very careful to interpret the latter as a real advantage of mSENSE. A closer look at the individual subjects revealed that one of the five investigated subjects at low spatial resolution showed generally quite weak and variable activation, while one other subject showed quite strong head motion in the questionable experiment, probably leading to the observed low *t*-value. Furthermore, the maximum *t*-value is also not an optimal indicator for the quality of fMRI experiments since, at least for a small number of subjects, it is certainly strongly influenced by chance, which is mirrored by the huge SDs over subjects. In adverse circumstances it might even be biased and overestimate the performance of an experiment with low SNR. Also, the investigated occipital primary visual cortex is only a part of the brain and different brain areas are affected quite differently by artifacts and additional noise amplification, as demonstrated by Schmidt et al (17). Therefore, our impression of an overall better performance of GRAPPA is not influenced too much by this incidental finding.

In conclusion, EPI with GRAPPA at a reduction factor of 2 revealed similar image quality than without parallel imaging, while temporal SNR and sensitivity toward functional activation were not affected significantly. This was true for low as well as high spatial resolution. Diffuse areas of increased noise amplification became only apparent at a reduction factor of 3, at which a marked sensitivity loss also occurred. mSENSE on the other hand, was generally more susceptible to residual unfolding artifacts than GRAPPA, and also exhibited, at least in our eyes, more unfavorable patterns of noise amplification in lateral brain areas even at R = 2. We would like to emphasize that this result is valid for the actual implementation of GRAPPA and mSENSE on our scanner and might differ for different implementations of those techniques in the future or from other vendors.

ACKNOWLEDGMENTS

We thank Arne Reykowski (Siemens Medical Solutions, Erlangen, Germany) for supplying maps of inverse *g*-factor of the eight-channel head coil, and the subjects who participated in this study.

REFERENCES

1. Norris DG. High field human imaging. J Magn Reson Imaging 2003; 18:519–529.
2. Hu X, Norris DG. Advances in high-field magnetic resonance imaging. Annu Rev Biomed Eng 2004;6:157–184.
3. Moelker A, Pattynama PM. Acoustic noise concerns in functional magnetic resonance imaging. Hum Brain Mapp 2003;20:123–141.
4. de Zwart JA, van Gelderen P, Kellman P, Duyn JH. Reduction of gradient acoustic noise in MRI using SENSE-EPI. Neuroimage 2002;16:1151–1155.
5. Blaimer M, Breuer F, Mueller M, Heidemann RM, Griswold MA, Jakob PM. SMASH, SENSE, PILS, GRAPPA: how to choose the optimal method. Top Magn Reson Imaging 2004;15:223–236.
6. Golay X, de Zwart JA, Ho YC, Sitoh YY. Parallel imaging techniques in functional MRI. Top Magn Reson Imaging 2004;15:255–265.
7. de Zwart JA, van Gelderen P, Golay X, Ikonomidou VN, Duyn JH. Accelerated parallel imaging for functional imaging of the human brain. NMR Biomed 2006;19:342–351.
8. Griswold MA, Jakob PM, Edelman RR, Sodickson DK. EPI acquisition strategies using SMASH. In: Proceedings of the 6th Annual Meeting of ISMRM, Sydney, Australia, 1998 (Abstract 423).
9. Griswold MA, Jakob PM, Chen Q, et al. Resolution enhancement in single-shot imaging using simultaneous acquisition of spatial harmonics (SMASH). Magn Reson Med 1999;41:1236–1245.
10. Weiger M, Pruessmann KP, Osterbauer R, Bornert P, Boesiger P, Jezzard P. Sensitivity-encoded single-shot spiral imaging for reduced susceptibility artifacts in BOLD fMRI. Magn Reson Med 2002;48:860–866.
11. de Zwart JA, van Gelderen P, Kellman P, Duyn JH. Application of sensitivity-encoded echo-planar imaging for blood oxygen level-dependent functional brain imaging. Magn Reson Med 2002;48: 1011–1020.
12. Schmidt CF, Degonda N, Henke K, Boesiger P. Application of SENSE to fMRI studies of higher cognitive functions. In: Proceedings of the 11th Annual Meeting of ISMRM, Toronto, Ontario, Canada, 2003 (Abstract 737).
13. Tang H, Tabert MH, Albers M, Devanand DP, Wu EX, Brown TR. An optimized EPI pulse sequence using SENSE for fMRI studies of orbitofrontal and medial temporal brain areas. In: Proceedings of the 12th Annual Meeting of ISMRM, Kyoto, Japan, 2004 (Abstract 1029).
14. Morgan PS, Kozel FA, George MS, Johnson KA, Baylis GC, Rorden C. Optimal SENSE factor for BOLD fMRI at 3T. In: Proceedings of the 12th Annual Meeting of ISMRM, Kyoto, Japan, 2004 (Abstract 1030).

15. Little MW, Papdaki A, McRobbie DW. An investigation of GRAPPA in conjunction with fMRI of the occipital cortex at 3 T. In: Proceedings of the 12th Annual Meeting of ISMRM, Kyoto, Japan, 2004 (Abstract 1025).
16. Tintera J, Gawehn J, Bauermann T, Vucurevic G, Stoeter P. New partially parallel acquisition technique in cerebral imaging: preliminary findings. Eur Radiol 2004;14:2273–2281.
17. Schmidt CF, Degonda N, Luechinger R, Henke K, Boesiger P. Sensitivity-encoded (SENSE) echo planar fMRI at 3T in the medial temporal lobe. Neuroimage 2005;25:625–641.
18. Sodickson DK, Manning WJ. Simultaneous acquisition of spatial harmonics (SMASH): fast imaging with radiofrequency coil arrays. Magn Reson Med 1997;38:591–603.
19. Pruessmann KP, Weiger M, Scheidegger MB, Boesiger P. SENSE: sensitivity encoding for fast MRI. Magn Reson Med 1999;42:952–962.
20. Wang J, Kluge T, Nittka M, Jellus V, Kühn B, Kiefer B. Parallel acquisition techniques with modified SENSE reconstruction mSENSE. In: Proceedings of the first Würzburg Workshop on Parallel Imaging Basics and Clinical Applications, Würzburg, 2001 (Abstract 89).
21. Griswold MA, Jakob PM, Heidemann RM, et al. Generalized autocalibrating partially parallel acquisitions (GRAPPA). Magn Reson Med 2002;47:1202–1210.
22. Griswold MA. Advanced k-space techniques. In: Proceedings of the 2nd International Workshop on Parallel MRI, Latsis Symposium, Zurich, 2004 (p. 16–18). October 15–17, 2004; ETH, Zurich, Switzerland. Sponsors: Foundation Latsis Internationale, GE Medical Systems, MRI Devices Corporation, Philips Medical Systems, Siemens Medical Systems, Toshiba Medical Systems.
23. Lutcke H, Merboldt KD, Frahm, J. The cost of parallel imaging in functional MRI of the human brain. Magn Reson Imaging 2006;24:1–5.
24. Schmidt CF, Pruessmann KP, Jaermann T, Lamerichs R, Boesiger P. High resolution fMRI using SENSE at 3 Tesla. In: Proceedings of the 10th Annual Meeting of ISMRM, Honolulu, HI, USA, 2002 (Abstract 125).
25. Hoogenraad F, Rijckaert Y, Harvey RP, Folkers P. High resolution ER-fMRI using SENSE at 3.0 T. In: Proceedings of the 10th Annual Meeting of ISMRM, Honolulu, HI, USA, 2002 (Abstract 126).
26. Preibisch C, Pilatus U, Bunke J, Hoogenraad F, Zanella F, Lanfermann H. Functional MRI using sensitivity-encoded echo planar imaging (SENSE-EPI). Neuroimage 2003;19:412–421.
27. Ohliger MA, Grant AK, Sodickson DK. Ultimate intrinsic signal-to-noise ratio for parallel MRI: electromagnetic field considerations. Magn Reson Med 2003;50:1018–1030.
28. Wiesinger F, Boesiger P, Pruessmann KP. Electrodynamics and ultimate SNR in parallel MR imaging. Magn Reson Med 2004;52:376–390.
29. Van de Moortele P, Adriany G, Moeller S, et al. Whole brain fMRI in human at ultra-high field with parallel SENSE imaging. In: Proceedings of the 12th Annual Meeting of ISMRM, Kyoto, Japan, 2004 (Abstract 1027).
30. Stenger VA, Noll DC, Boada FE. Partial Fourier reconstruction for three-dimensional gradient echo functional MRI: comparison of phase correction methods. Magn Reson Med 1998;40:481–490.
31. Griswold MA, Breuer F, Blaimer M, et al. Autocalibrated coil sensitivity estimation for parallel imaging. NMR Biomed 2006;19:316–324.
32. Griswold MA, Kannengiesser S, Heidemann RM, Wang J, Jakob PM. Field-of-view limitations in parallel imaging. Magn Reson Med 2004;52:1118–1126.
33. Kruger G, Glover GH. Physiological noise in oxygenation-sensitive magnetic resonance imaging. Magn Reson Med 2001;46:631–637.
34. Kruger G, Kastrup A, Glover GH. Neuroimaging at 1.5 T and 3.0 T: comparison of oxygenation-sensitive magnetic resonance imaging. Magn Reson Med 2001;45:595–604.